AGU PUBLICATIONS

Geophysical Research Letters

RESEARCH LETTER
10.1002/2015GL063390

Key Points:
- Discovery and in situ survey of a subglacial lake in central West Antarctica
- The lake is very likely a system with long water residence time
- The lake is a new, privileged site for glaciological and biological research

Correspondence to:
A. Rivera,
arivera@cecs.cl

Citation:
Rivera, A., J. Uribe, R. Zamora, and J. Oberreuter (2015), Subglacial Lake CECs: Discovery and in situ survey of a privileged research site in West Antarctica, *Geophys. Res. Lett.*, *42*, 3944–3953, doi:10.1002/2015GL063390.

Received 6 FEB 2015
Accepted 19 APR 2015
Accepted article online 22 APR 2015
Published online 21 MAY 2015

Subglacial Lake CECs: Discovery and in situ survey of a privileged research site in West Antarctica

Andrés Rivera[1,2], José Uribe[1], Rodrigo Zamora[1], and Jonathan Oberreuter[1]

[1]Centro de Estudios Científicos, Valdivia, Chile, [2]Departamento de Geografía, Universidad de Chile, Santiago, Chile

Abstract We report the discovery and on-the-ground radar mapping of a subglacial lake in Antarctica, that we have named Lake CECs (Centro de Estudios Científicos) in honor of the institute we belong to. It is located in the central part of the West Antarctic Ice Sheet, right underneath the Institute Ice Stream and Minnesota Glacier ice divide, and has not experienced surface elevation changes during the last 10 years. The ratio between the area of the subglacial lake and that of its feeding basin is larger than those for either subglacial lakes Ellsworth or Whillans, and it has a depth comparable to that of Ellsworth and greater than that of Whillans. Its ice thickness is ~600 m less than that over Ellsworth. The lake is very likely a system with long water residence time. The recent finding of microbial life in Lake Whillans emphasizes the potential of Subglacial Lake CECs for biological exploration.

1. Introduction

Subglacial lakes are recognized as important components of the complex hydrological system that exists at the base of the Antarctic Ice sheet, where circulation of basal meltwater plays a key role in ice stream dynamics [*Wright et al.*, 2008]. Up to now 379 potential subglacial lakes have been identified [*Wright and Siegert*, 2012], very few of them at the center of the West Antarctic Ice Sheet (WAIS). Nearly 150 of these potential lakes lack confirmation by in situ measurements, and in some cases, when detailed radar surveys were performed, the results did not show the expected subglacial lake signals [*Siegert et al.*, 2014]. The scarcity of subglacial lakes in the central part of West Antarctica contrasts with the presence of many in central East Antarctica, where the bedrock is deep enough for melting to take place at the ice bottom and where the slope of the bedrock relief is able to trap subglacial water [*Tabacco et al.*, 2006]. In West Antarctica the great majority of the already identified subglacial lakes are active and are located near the outlet of fast ice flow regions or in the tributary regions feeding them [*Smith et al.*, 2009]. In the upper central part of West Antarctica, only Subglacial Lake Ellsworth has been described up to now [*Vaughan et al.*, 2007], but others might have remained undetected for lack of detailed surveys.

WAIS is considered potentially unstable because its bed is well below sea level and its total disintegration could contribute up to 4.3 m to global sea level rise [*Fretwell et al.*, 2013]. The ice divide between the Amundsen and Weddell seas at the center of WAIS has been described as stable over the last thousands of years [*Ross et al.*, 2011]. This stability might be altered as a consequence of the changes taking place in recent decades at the lower end of Pine Island Glacier (PIG) that are currently spreading upstream, a process illustrated by the grounding line migration of nearly 31 km along the main ice plain [*Rignot et al.*, 2011a, 2014]. The data required to address the stability issue at this ice divide (Figure 1), especially between PIG, Rutford (RUT), Minnesota (MIN), and Institute (IIS), are very scarce [*Ross et al.*, 2012, 2013], in particular, because InSAR-derived ice velocities are poorly constrained [*Rignot et al.*, 2011b]. To help fill these gaps we conducted in January 2014 a 1200 km radar traverse to this area departing from Union Glacier [*Rivera et al.*, 2014].

2. Methods

The oversnow traverse was carried out in January 2014 from our mobile research station which operates out of Union Glacier. The station is equipped to conduct radar measurements of ice thickness using a coherent pulse compression radar designed at Centro de Estudios Científicos (CECs) [*Uribe et al.*, 2014]. The system transmits with a peak power of 200 W working at a central frequency of 155 MHz and a bandwidth of 20 MHz. It operates at a pulse repetition frequency (PRF) of 10 kHz. The receiver uses high- and low-signal amplification

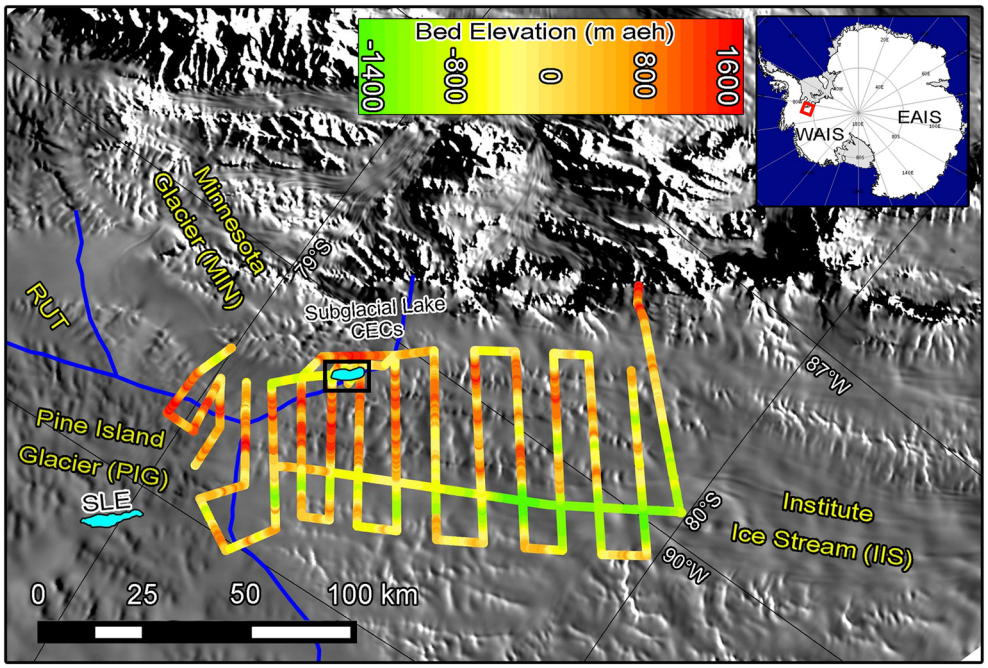

Figure 1. Study area in WAIS. Ice divides (blue lines), subglacial lakes (light blue polygons), and surveyed tracks (color scale) are shown. Black box shows the location of Figure 2 (top). RUT: Rutford Ice Stream. SLE: Subglacial Lake Ellsworth. Background image: Moderate Resolution Imaging Spectroradiometer (MODIS) mosaic [*Scambos et al.*, 2007].

channels; the low-gain channel was useful to penetrate shallow ice (<1 km depth), and the high-amplification channel was capable of measuring deeper ice (up to 4 km depth). Both channels are combined in postprocessing for better radargram visualization, where a vertical resolution of 5 m was achieved. The upper 200 m of snow and firn layers were mapped with a vertical resolution of 0.2 m using a Frequency-Modulated Continuous-Wave (FMCW) radar also designed at CECs operating at frequencies between 203 and 1019 MHz. This system uses two separate log periodic antennae for the transmitter and receiver. It has a peak power of 250 mW and a PRF of 5.5 kHz. The radar data were geolocated using dual-frequency Lexon GD GPS receivers. Background removal, dewow filter, and adjustment of the gain function were applied to the raw radar data. Coherent integration (2048 traces) was applied to the raw radar data (unfocused SAR) to reduce oblique scattering, improve along-track resolution, and increase signal-to-noise ratio. In order to convert travel time to ice thickness, an electromagnetic wave velocity propagation through the ice of 0.168 m ns^{-1} was assumed. Kirchhoff migration was applied to the radar data before manual picking. The bottom reflections were manually picked using REFLEXW Software. The errors in ice thickness measurements stem from ice/snow density variations, uncertainties in identifying the onset of the bottom reflections, GPS position, and vertical radar resolution. In the absence of direct measurements of some of the above parameters, we estimated those errors through crossover analysis of the entire survey. The variations between different survey tracks turn out to be less than 5% in ice thickness and less than 20 cm in ice surface topography. The survey pattern was designated to perpendicularly cross the troughs that span from the Ellsworth Mountains to the south. These subglacial valleys are important inception areas for downstream fast ice flow [*Ross et al.*, 2013]. The radar survey aimed to map the difference in bedrock between the hard bedrock hanging valleys and the lower soft valley bottoms.

3. Results and Discussion

3.1. Topographic Setting

Along our 14 day traverse that took place during January 2014, we detected a subglacial lake (named CECs, Centro de Estudios Científicos) that is confined by prominent bedrock steep-sided walls, within a region with complex subglacial topography that has a maximum ice thickness of 3.1 km. This complex topography comprised rough subglacial features, including deep valleys with soft beds, separated by steep flanks with several hanging tributaries connecting Ellsworth Trough (ET) with other semiparallel troughs (such as T1 in *Ross et al.* [2013]).

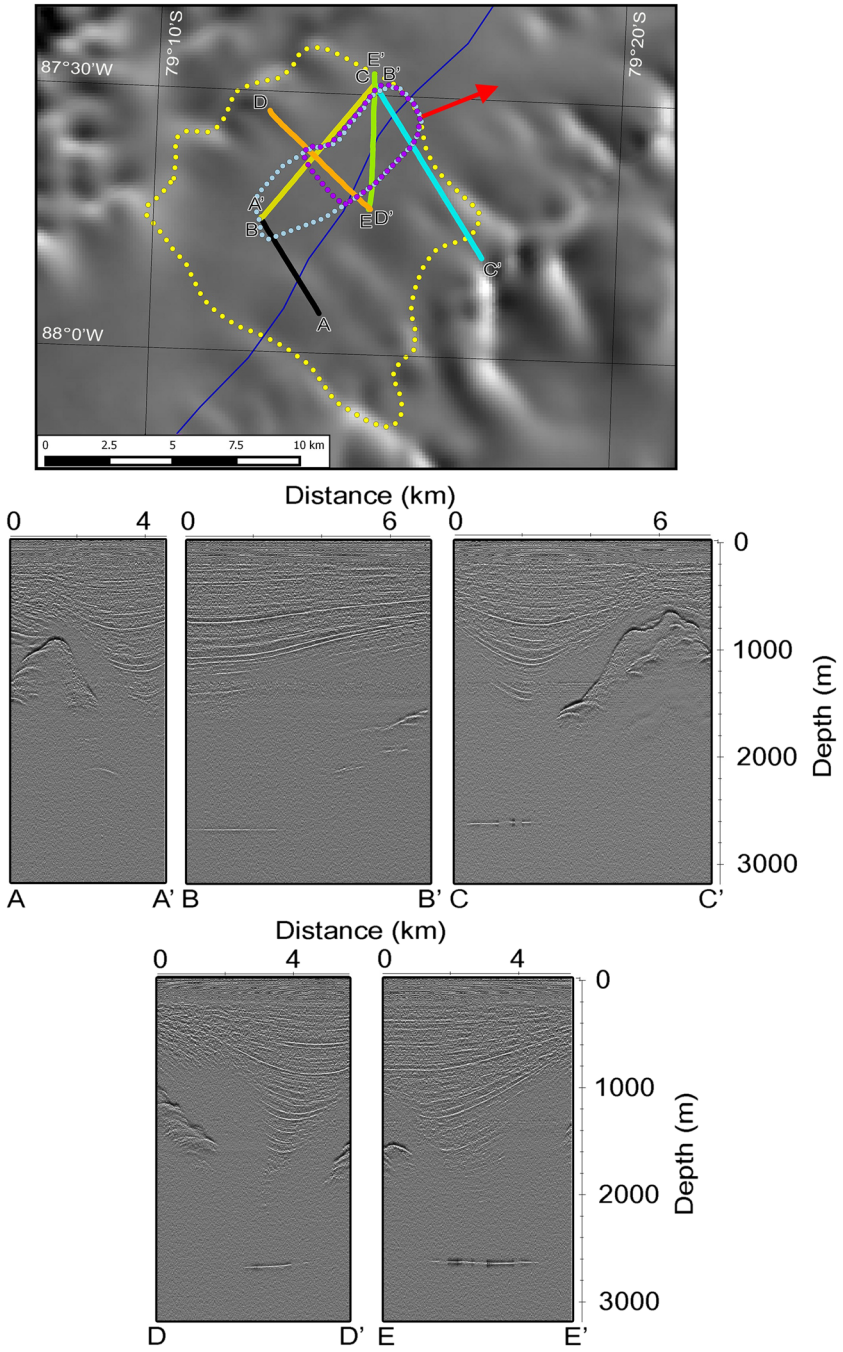

Figure 2. (top) Location of the radar profiles described in Figure 2 (bottom) and in Figures 3 and 4 (Background image MODIS mosaic [*Scambos et al.*, 2007]). Yellow dots: *H* basin. Light blue dots: Subglacial Lake CECs. Purple dots: deeper than 10 m Subglacial Lake CECs. Dark blue: Ice divide between Minnesota Glacier (MIN) and Institute Ice Stream (IIS). Red arrow: direction of potential lake outflow path (Maximum *H* downstream slope). (bottom) Two-dimensional nonmigrated diagrams with profiles AA′, BB′, CC′, DD′, and EE′.

At the ice divide between IIS and MIN (79°15′S 87°34′W), between two parallel subglacial ranges, a bright bed reflection signal with the distinctive signature of subglacial lake returns [*Oswald and Robin*, 1973] was observed. This flat and bright feature with strong power reflections appeared to be surrounded by very rough subglacial topography with peaks at hundreds of meters above the bright reflector, reminiscent of the geomorphology of a deep subglacial fjord-like valley or trough. Figure 2 shows some of these radar profiles where the flat returns are surrounded by peaks of 1000 m above the bottom. Between the crest and the bottom,

the radar returns disappear due to steep slopes (Figure 2). The isochronous layers above the flat reflectors are inflected toward the bottom, indicating melting at the bed. The sensitivity of the radar was not good enough to detect accretion ice or layers down to the lake surface.

The parameters which are used to discern the presence of a subglacial lake are the following: ice sheet topography slope, surface slope versus ice thickness relationship, hydrological head (H), Bed Reflection Power (BRP), and BRP specularity [*Vaughan et al.*, 2007; *Kapitsa et al.*, 1996; *Carter et al.*, 2007]. In three of the radar profiles (Figure 3, CC′, DD′, and EE′) all the conditions for the presence of a subglacial lake were satisfied, namely: very smooth ice sheet surface topography; surface slope versus ice thickness relationship of 1/11; almost constant hydrological head, H; BRP values that were at least 15–20 dB higher than the returns from the surrounding rock or sediments; low-specularity BRP, i.e., the reflection power varying by less than 50% from the mean reflection strength over any given 300 m continuous subset of samples within the lake candidate.

The conditions described above are those of subglacial lakes whose water depth is greater than 10 m [*Siegert et al.*, 2014]. The subglacial lake conditions are fully realized over an estimated area of ~12 km^2 as shown in profiles CC′, DD′, and EE′ (purple dots in Figure 2). Immediately upstream, a fourth profile (BB′) shows similar parameter values but with *H* differing by about 1 m (yellow dots in Figure 4). This difference can be due to higher water density or, more likely, to returns coming from shallow waters or from water-embedded marine sediments [*Kapitsa et al.*, 1996]. This contiguous area has ~6 km^2, giving a figure of near 18 km^2 for the total area of Subglacial Lake CECs (light blue dots in Figure 2) and a mean altitude of 626 m below ellipsoidal height. The ice sheet surface topography above the lake is very smooth with a mean altitude of 2029 ± 3 m above ellipsoid height (aeh).

3.2. Water Properties

Considering a mean thickness of 2653 m of ice above the lake, we estimate a melting pressure point of −1.8°C at the boundary layer between the subglacial lake and the overlaying ice. The mean ice density above the lake is unknown, but assuming that our radar data show that only the upper 200 m is composed of snow/firn and that the densities in deeper ice in the Antarctic ice sheet are close to the theoretical maximum, we can preliminarily define a range of ice densities between 910 and 920 kg m^{-3} [*Cuffey and Paterson*, 2010]. Using this range, the fluid density at the lake can be calculated [*Vaughan et al.*, 2007], resulting in values from 1004 to 1015 kg m^{-3}. Considering that the lake is under an overburden pressure of near 24 MPa, this density range should be considered typical of a fresh water body (black line in Figure 4). Similar density characteristics were found on Subglacial Lake Ellsworth that is under an overburden pressure of 28 MPa, also considered a fresh water body [*Vaughan et al.*, 2007]. Since the ice above Lake CECs is thinner than 3050 m, it must be considered a stratified water body, following the criteria proposed by *Thoma et al.* [2011].

3.3. Subglacial Lake Stability

Assuming that the presence of conduits in the ice are unlikely and that the ice above the lake is fully supported by the pressure of the fluid in the lake, the hydrological head *H* on the deeper side has a mean value of 1778 ± 0.5 m (minimum ΔH_{RMS}). This value for *H* was obtained using a mean ice density of 915 kg m^{-3} and a mean fluid density of 1010 kg m^{-3}, (black line in Figure 4). The *H* values in the area immediately surrounding the lake are much higher than those at the lake, except toward the south where *H* is only 5 m greater. Beyond this threshold (southward, red arrow in Figure 2), *H* decreases continuously, indicating that any eventual water outflow from the lake would follow this path toward IIS. Some subglacial lakes in Antarctica have shown this kind of drainage even with less than 5 m difference of *H* [*Christianson et al.*, 2012], and in some cases they have steadily inflated during short periods of time [*Smith et al.*, 2009].

A stable subglacial lake is a repository of geological and biological information over an extended continuous time line, which makes the case for its study compelling. In order to evaluate the stability of the lake, we have analyzed two key independent parameters, the vertical movement of the ice sheet surface and the melting rate at the bottom of the ice sheet. Our conclusion as discussed below is that the lake is quite stable.

We first address the issue of vertical movement. Available ICESat data collected from two tracks repeatedly measured between October 2003 and March 2009, showed vertical differences of less than 0.5 m along the subglacial lake CECs area, a figure that is at least less than one third of that associated with lakes that have outflows [*Siegert et al.*, 2014]. This is already a significant indication of stability, as the estimated errors of ICESat data are in the order of few centimeters per year [*Borsa et al.*, 2014].

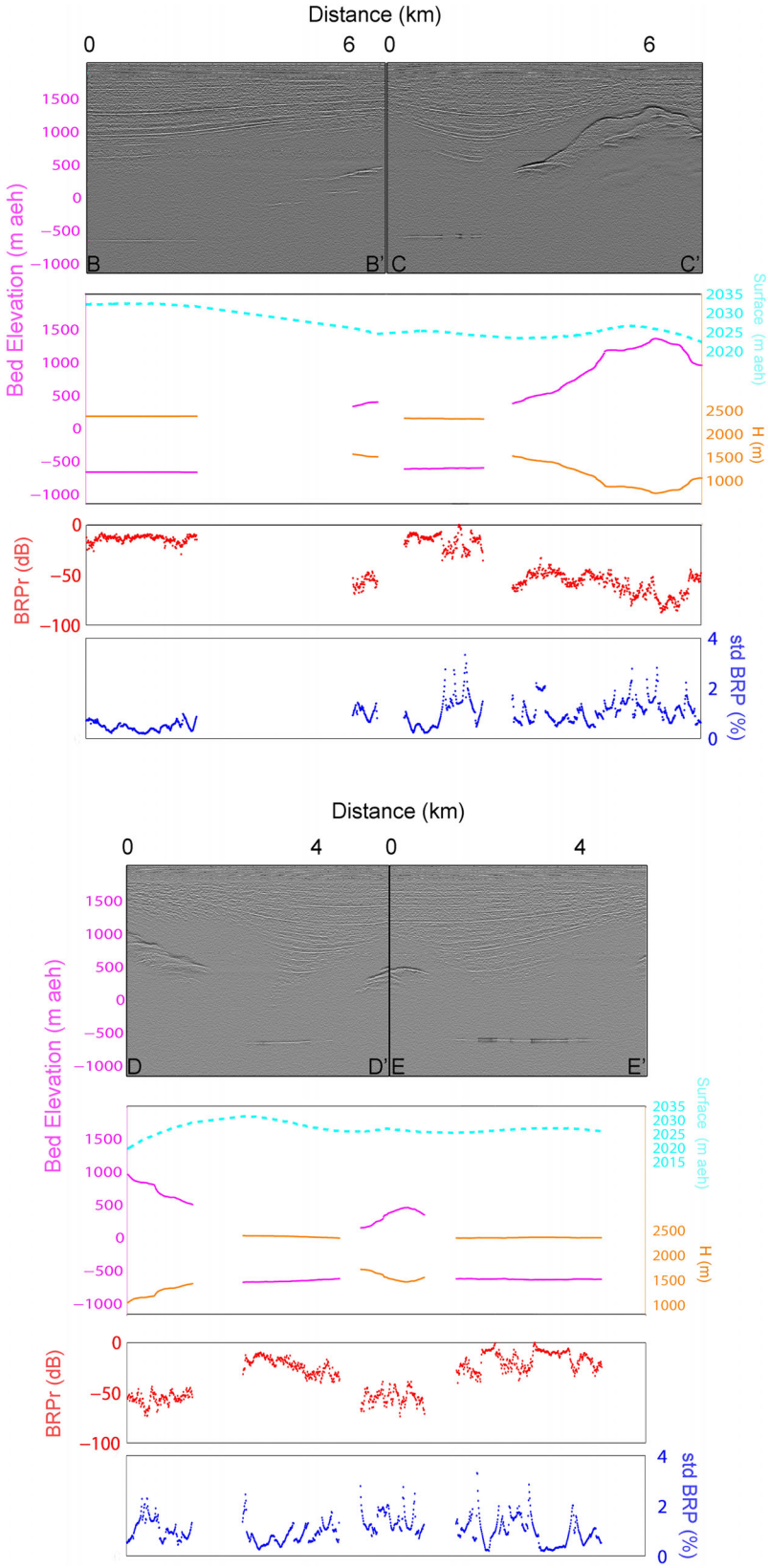

Figure 3. (from top to bottom) Nonmigrated radar data, ice sheet surface topography (magenta), subglacial topography (cyan), hydrological head (orange), Bed Reflection Power (BRP in red), and BRP specularity (std BRP in blue) from the subglacial lake (Profiles BB′, CC′, DD′, and EE′). (See location of each profile in Figure 2).

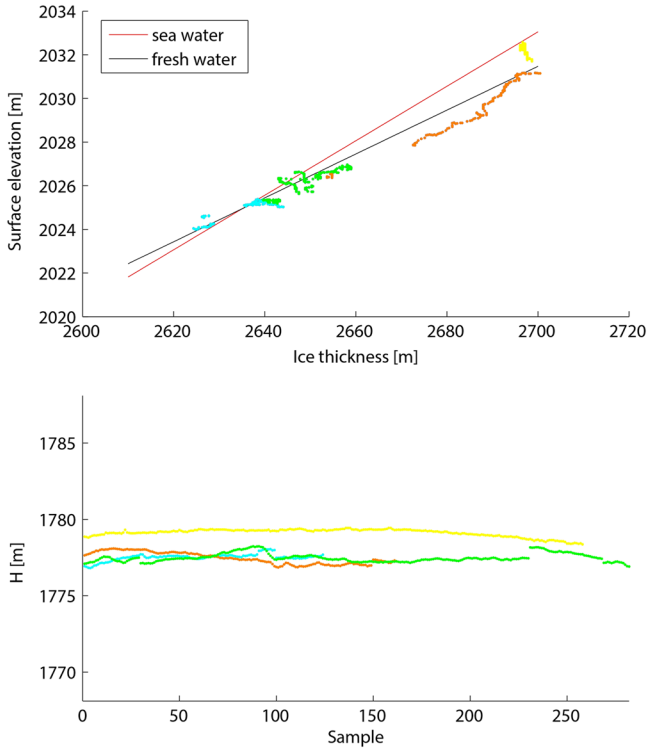

Figure 4. (top) Estimated lake water densities versus ice thickness. (bottom) Hydrological head for each radar profile with lake-like returns (see Figure 2 for location of each radar profile).

To further analyze the issue, one may assume that the lake had an outflow and calculate the volume of water needed to increase the lake level by 5 m in order to surpass the *H* threshold. The resulting figure is 0.09 km^3 (vertical height of 0.005 km times 18 km^2). If it existed, this extra water volume could be originated by melting at the bottom of the ice, coming from a feeding subglacial drainage area of ~110 km^2 (yellow dot line in Figure 2); however, a more intensive survey needs to be done to better constrain its size. This subglacial basin is very steep toward the lake surface, with similar slopes to those observed at Subglacial Lake Ellsworth [*Bamber et al.*, 2013]. The subglacial basin was delineated using all available *H* values (calculated using equation (A10) in Appendix A) and following the methods described by *Bamber et al.* [2013]. These *H* values were overlapped and compared to the Moderate Resolution Imaging Spectroradiometer Mosaic of Antarctica (MODIS MOA) 2004 [*Scambos et al.*, 2007], allowing a better delineation of the subglacial basin. This mosaic has been already used to interpret subglacial features, since basal morphology influences ice surface elevation patterns as observed by MODIS [*Ross et al.*, 2013]. The melting rate at the basin bed is highly dependent on the geothermal heat flux, that at the center of WAIS (underneath Thwaites) ranges from a mean minimum of 114 ± 10 mW m^{-2} [*Schroeder et al.*, 2014] to a maximum of 240 mW m^{-2} at the continental ice divide [*Clow et al.*, 2012]. The geothermal source of energy at a subglacial lake is partially used as latent heat (for melting the ice), and the rest is conducted toward the ice surface. Assuming this geothermal heat flux range plus a surface ice accumulation of 0.17 m yr^{-1} [*Siegert et al.*, 2004], a surface temperature of −25°C and the ice thickness estimated from our data for the whole basin, we can estimate that the melting at the bottom of the ice overlaying the subglacial lake basin is between 6.5 and 19.7 mm yr^{-1}.

With this melt rate range at the subglacial basin, the increase in volume needed to trigger an outflow would require a time period of several decades, which in turn indicates that the water balance within the lake is likely achieved by accretion ice, a process for which there are precedents [*Jouzel*, 1999].

At least four active subglacial lakes have been recently detected near IIS grounding line zone [*Siegert et al.*, 2014]. These lower altitude subglacial lakes are receiving melt water from a wide and vast basin extended as far as the ice divide between PIG and IIS. The water pathway between this continental divide, where Subglacial Lake CECs is located, and the grounding line zone of IIS comprised several valleys excavated by former local glaciers that overdeepened tectonic features existing in parallel to the Ellsworth Mountains [*Ross et al.*, 2013].

The fastest ice flow of IIS takes place along these U-shaped subglacial valleys, especially the so-called Ellsworth Trough where maximum ice velocities reach 75 m yr^{-1} near the Ellsworth Mountains [*Rignot et al.*, 2011a]. The presence of Subglacial Lake CECs at the inception of one of the fastest arms of the Institute Ice Stream potentially has an important role in its ice dynamic. A similar link has been observed by *Bell et al.* [2007] at Recovery Glacier Ice Stream. Since no overflows originating from Lake CECs have been observed with the available data, a midterm monitoring program is highly desirable.

4. Conclusions

We have reported the discovery and on-the-ground radar mapping of Subglacial Lake CECs, a previously uncharted body of water located right at the ice divide between the Institute Ice Stream and the Minnesota Glacier, in the central part of West Antarctica. This lake possesses properties which existing together make it quite unique and comparatively advantageous over subglacial lakes Ellsworth [*Vaughan et al.*, 2007] and Whillans [*Tulaczyk et al.*, 2014] as a subject of exploration in West Antarctica. Subglacial Lake CECs contains fresh water. It has an estimated area of near 18 km^2, located at −626 m aeh, beneath 2653 m of ice. The comparison of available ICESat data from the ice sheet surface above the lake does not show recent vertical displacements. Therefore, the lake is very likely a system with long water residence time in the order of tens of years; however, its position at the inception of IIS converts it in a potentially important triggering ice dynamic factor.

Appendix A: Supplementary Information

The vertical velocity at the accumulation zone of a glacier can be approximated to

$$w = -\frac{bz}{E} \tag{A1}$$

where b is the ice accumulation rate (0.17 m yr^{-1} [*Siegert et al.*, 2004]) and E is the ice thickness (2653 m).

The temperature at the base of the ice sheet can be formulated as follows:

$$T_B = T_S - \left[\frac{dT}{dz}\right]_B \int_0^E e^{-z^2/\zeta^2} dz \tag{A2}$$

where T_B is the basal temperature, T_S the surface temperature (−25°C), $[dT/dz]_B$ is the temperature gradient at the glacier base:

$$\left[\frac{dT}{dz}\right]_B = -\frac{q}{K} \tag{A3}$$

where q is the heat flux at the glacier bed (that could be equal to the geothermal flux if there is no melting) and K is the thermal conductivity of the ice. Also, we can write

$$\zeta^2 = \frac{2\alpha_T E}{b} \tag{A4}$$

where α_T is the thermal diffusivity of the ice (37.2 m^2 yr^{-1} [*Hooke*, 2005]).

Considering that the subglacial lake is at the ice divide between Institute Ice Stream and Minnesota Glacier, we can follow [*Raymond*, 1983], who defined the vertical velocity at an ice divide as follows:

$$w = \frac{-bz^2}{E^2} \tag{A5}$$

In this case, we can write

$$T_B = T_S - \left[\frac{dT}{dz}\right]_B \int_0^E e^{-z^3/\zeta^3} dz \tag{A6}$$

where

$$\zeta^3 = \frac{3\alpha_T E^2}{b} \tag{A7}$$

At the lake surface, the water temperature must be at the pressure melting point. Assuming a mean ice thickness above the lake of 2653 m, the pressure at the base must be

$$P = \rho_i g E \tag{A8}$$

where ρ_i is the ice density and g the gravity acceleration constant. Using $\rho_i = 915$ kg m^{-3}, $E = 2653$ m, and $g = 9.8$ m s^{-2}, P is 23.78 MPa and $\Delta P/\Delta T = -13.5$ MPa K^{-1}. Therefore, the melting pressure point is −1.8°C.

At the subglacial lake, part of the geothermal heat is used as latent heat (for melting the ice), and the rest of the energy is conducted toward the ice surface. Then, the basal melting can be calculated [*Hooke*, 2005] by

$$\frac{dm}{dt} = \left(\frac{K}{L}\right)\left(\left[\frac{dT}{dz}\right]_G - \left[\frac{dT}{dz}\right]_B\right) \tag{A9}$$

$K/L \cong 220$, where L is the latent water melting heat. Using equations (A6) and (A7), it is possible to calculate $[dT/dz]_B$.

The hydrological head H was calculated using [*Vaughan et al.*, 2007]:

$$H = \frac{\rho_i}{\rho_f} h_i + \frac{\rho_f - \rho_i}{\rho_f} z_b \tag{A10}$$

where ρ_i is the ice density (915 kg m^{-3}), ρ_f is the subglacial lake water density, h_i is the ice surface, and z_b is the subglacial lake surface elevation calculated as $z_b = h_i - E$, where E is the ice thickness. The ρ_f was estimated by minimizing the RMS differences of H (ΔH_{RMS}) assuming that H must be near constant on a subglacial lake surface [*Oswald and Robin*, 1973].

In the calculation of the Bed Reflection Power (BRP) we followed [*Gades et al.*, 2000]

$$\mathrm{BRP} = \frac{1}{n_2 - n_1 + 1} \sum_{n=n_1}^{n_2} {s_n}^2 \tag{A11}$$

where s_n is the radar signal amplitude received at each point; n_1 and n_2 are the beginning and end sample numbers of the calculation window (9 samples in our case).

For BRP calculation, it is necessary to compensate the effect of geometrical spreading of the radar signal and the dielectric attenuation in ice. With this corrected BRP, we can infer basal conditions beneath the glacier.

The corrected BRP is obtained as follows:

$$\mathrm{BRP}_R = \frac{\mathrm{BRP}}{\mathrm{BRP}_e} \tag{A12}$$

where BRP_R is the corrected BRP and BRP_e is the estimated BRP. The BRP_e does not consider the basal condition changes and can be obtained through an empirical model from a selected data set or from a theoretical model using the radar equation. We used the theoretical form due to large variability of the BRP obtained values.

An expression for the radar equation is

$$P_{rx} = P_{tx} G L_g T_{12}^2 L_i^2 R_{23} \tag{A13}$$

where P_{rx} is the received power, P_{tx} is the transmitted power (53 dBm), G is the total combinations of gains and losses from the radar system (about 60), L_g is the geometrical spreading loss, T_{12} is the transmission loss at the air-ice boundary (0.8 [*Bentley et al.*, 1998]), L_i is the dielectric loss in the ice column, and R_{23} is the power reflection coefficient of the bottom.

To get BRP_e, we can write

$$\mathrm{BRP}_e = P_{tx} G L_g T_{12}^2 L_i^2 \tag{A14}$$

The geometrical spreading loss is obtained using [*Bentley et al.*, 1998]

$$L_g = \frac{\lambda^2 G_a^2}{\left[\frac{8\pi E}{\sqrt{\epsilon_i}}\right]^2} \tag{A15}$$

where λ is the wavelength of the radar signal at the air medium (1.935 m), E is the ice thickness, ϵ_i is the relative electric permitivity of the ice (3.188 [*Glen and Paren*, 1975]), and G_a is the antenna gain (12 dBi).

We can obtain the dielectric loss in ice using [*Peters et al.*, 2005]

$$L_i = e^{-2\pi E \tan(\delta)/\lambda_i} \tag{A16}$$

where $\tan(\delta)$ is the loss tangent of the ice (0.0007 [*Evans*, 1965]) and λ_i is the wavelength of the radar signal in the ice medium (1.084 m).

Standard deviation of the BRP was obtained using [*Carter et al.*, 2007]:

$$\text{std\_BRP} = \frac{\text{std}(\text{BRP}_R)}{\text{mean}(\text{BRP}_R)} \tag{A17}$$

We used a calculation window of 20 samples, which corresponds to a measured distance of 200 m.

Acknowledgments

The radar data used to generate the diagrams and graphs for this paper are available at http://www.cecs.cl/files/RadarDataSLC.html. CECs is funded by the Base Finance program of CONICYT. The support of Antarctic Logistics and Expeditions (ALE) is gratefully acknowledged. Tobias Kohoutek and Ryan Wilson helped with GPS and ICESat data processing, and Francisco V. Sepúlveda with manuscript preparation. Thanks to Mike Sharp, Mike and Peter McDowell, Chris Jacobs, Boris Mihovilovic, Thomas Nonis, and all ALE personnel at Union Glacier. This research would have not been possible without the permanent support of Claudio Bunster, CECs director.

The Editor thanks two anonymous reviewers for their assistance in evaluating this paper.

References

Bamber, J., M. Siegert, J. Griggs, S. Marshall, and G. Spada (2013), Paleofluvial Mega-Canyon beneath the central Greenland ice sheet, *Science*, *341*, 997–999.

Bell, R. E., M. Studinger, C. A. Shuman, M. A. Fahnestock, and I. Joughin (2007), Large subglacial lakes in East Antarctica at the onset of fast-flowing ice streams, *Nature*, *445*, 904–907.

Bentley, C. R., N. Lord, and C. Liu (1998), Radar reflections reveal a wet bed beneath stagnant ice stream C and a frozen bed beneath ridge BC, West Antarctica, *J. Glaciol.*, *44*(146), 149–156.

Borsa, A., G. Moholdt, H. Fricker, and K. Brunt (2014), A range correction for ICESat and its potential impact on ice sheet mass balance studies, *Cryosphere*, *8*, 345–357.

Carter, S. P., D. D. Blankenship, M. E. Peters, D. A. Young, J. W. Holt, and D. L. Morse (2007), Radar-based subglacial lake classification in Antarctica, *Geochem. Geophys. Geosyst.*, *8*, Q03016, doi:10.1029/2006GC001408.

Christianson, K., R. W. Jacobel, H. J. Horgan, S. Anandakrishnan, and R. B. Alley (2012), Subglacial Lake Whillans—Ice-penetrating radar and GPS observations of a shallow active reservoir beneath a West Antarctic ice stream, *Earth Planet. Sc. Lett.*, *331–332*, 237–245.

Clow, G. D., K. M. Cuffey, and E. D. Waddington (2012), High heat-flow beneath the central portion of the West Antarctic Ice Sheet, Abstract C31A-0577 paper presented at 2012 Fall Meeting, AGU, San Francisco, Calif., 3–7 Dec.

Cuffey, K., and W. Paterson (2010), *The Physics of Glaciers*, 4th ed., Elsevier, Burlington.

Evans, S. (1965), Dielectric properties of ice and snow—A review, *J. Glaciol.*, *5*(42), 773–792.

Fretwell, P., et al. (2013), Bedmap2: Improved ice bed, surface and thickness datasets for Antarctica, *Cryosphere*, *7* (1), 375–393, doi:10.5194/tc-7-375-2013.

Gades, A., C. Raymond, H. Conway, and R. Jacobel (2000), Bed properties of Siple Dome and adjacent ice streams, West Antarctica, inferred from radio-echo sounding measurements, *J. Glaciol.*, *46*(152), 88–94, doi:10.3189/172756500781833467.

Glen, J. W., and J. G. Paren (1975), The electrical properties of snow and ice, *J. Glaciol.*, *15*(73), 15–38.

Hooke, R. L. (2005), *Principles of Glacier Mechanics*, Cambridge Univ. Press, Cambridge, U. K., doi:10.1017/CBO9780511614231.

Jouzel, J. (1999), More than 200 meters of lake ice above Subglacial Lake Vostok, Antarctica, *Science*, *286*(5447), 2138–2141, doi:10.1126/science.286.5447.2138.

Kapitsa, A. P., J. K. Ridley, G. de Q. Robin, M. J. Siegert, and I. A. Zotikov (1996), A large deep freshwater lake beneath the ice of central East Antarctica, *Nature*, *381*(6584), 684–686, doi:10.1038/381684a0.

Oswald, G. K. A., and G. D. Q. Robin (1973), Lakes beneath the Antarctic Ice Sheet, *Nature*, *245*(5423), 251–254, doi:10.1038/245251a0.

Peters, M., D. Blankenship, and D. Morse (2005), Analysis techniques for coherent airborne radar sounding: Application to West Antarctic ice streams, *J. Geophys. Res.*, *110*, B06303, doi:10.1029/2004JB003222.

Raymond, C. (1983), Deformation in the vicinity of ice divides, *J. Glaciol.*, *29*(103), 357–373.

Rignot, E., J. Mouginot, and B. Scheuchl (2011a), Antarctic grounding line mapping from differential satellite radar interferometry, *Geophys. Res. Lett.*, *38*, L10504, doi:10.1029/2011GL047109.

Rignot, E., J. Mouginot, and B. Scheuchl (2011b), Ice flow of the Antarctic ice sheet, *Science*, *333* (6048), 1427–1430, doi:10.1126/science.1208336.

Rignot, E., J. Mouginot, M. Morlighem, H. Seroussi, and B. Scheuchl (2014), Widespread, rapid grounding line retreat of Pine Island, Thwaites, Smith, and Kohler glaciers, West Antarctica, from 1992 to 2011, *Geophys. Res. Lett.*, *41*, 3502–3509, doi:10.1002/2014GL060140.

Rivera, A., R. Zamora, J. A. Uribe, R. Jaña, and J. Oberreuter (2014), Recent ice dynamic and surface mass balance of Union Glacier in the West Antarctic Ice Sheet, *Cryosphere*, *8*(4), 1445–1456, doi:10.5194/tc-8-1445-2014.

Ross, N., M. J. Siegert, J. Woodward, A. M. Smith, H. F. J. Corr, M. J. Bentley, R. C. A. Hindmarsh, E. C. King, and A. Rivera (2011), Holocene stability of the Amundsen-Weddell ice divide, West Antarctica, *Geology*, *39*(10), 935–938, doi:10.1130/G31920.1.

Ross, N., R. G. Bingham, H. F. J. Corr, F. Ferraccioli, T. A. Jordan, A. Le Brocq, D. M. Rippin, D. Young, D. D. Blankenship, and M. J. Siegert (2012), Steep reverse bed slope at the grounding line of the Weddell Sea sector in West Antarctica, *Nat. Geosci.*, *5* (6), 393–396, doi:10.1038/ngeo1468.

Ross, N., T. A. Jordan, R. G. Bingham, H. F. J. Corr, F. Ferraccioli, A. Le Brocq, D. M. Rippin, A. P. Wright, and M. J. Siegert (2013), The Ellsworth subglacial highlands: Inception and retreat of the West Antarctic Ice Sheet, *Geol. Soc. Am. Bull.*, *126*(1–2), 3–15, doi:10.1130/B30794.1.

Scambos, T., T. Haran, M. Fahnestock, T. Painter, and J. Bohlander (2007), MODIS-based Mosaic of Antarctica (MOA) data sets: Continent-wide surface morphology and snow grain size, *Remote Sens. Environ.*, *111*(2–3), 242–257, doi:10.1016/j.rse.2006.12.020.

Schroeder, D. M., D. D. Blankenship, D. A. Young, and E. Quartini (2014), Evidence for elevated and spatially variable geothermal flux beneath the West Antarctic Ice Sheet, *Proc. Natl. Acad. Sci. U.S.A.*, *111*(25), 9070–9072, doi:10.1073/pnas.1405184111.

Siegert, M. J., R. Hindmarsh, H. Corr, A. Smith, J. Woodward, E. C. King, A. J. Payne, and I. Joughin (2004), Subglacial lake Ellsworth: A candidate for in situ exploration in West Antarctica, *Geophys. Res. Lett.*, *31*, L23403, doi:10.1029/2004GL021477.

Siegert, M. J., N. Ross, H. Corr, B. Smith, T. Jordan, R. G. Bingham, F. Ferraccioli, D. M. Rippin, and A. Le Brocq (2014), Boundary conditions of an active West Antarctic subglacial lake: Implications for storage of water beneath the ice sheet, *Cryosphere*, *8*(1), 15–24, doi:10.5194/tc-8-15-2014.

Smith, B. E., H. A. Fricker, I. R. Joughin, and S. Tulaczyk (2009), An inventory of active subglacial lakes in Antarctica detected by ICESat (2003–2008), *J. Glaciol.*, *55*(192), 573–595.

Tabacco, I., P. Cianfarra, A. Forieri, F. Salvini, and A. Zirizotti (2006), Physiography and tectonic setting of the subglacial lake district between Vostok and Belgica subglacial highlands (Antarctica), *Geophys. J. Int.*, *165*(3), 1029–1040.

Thoma, M., K. Grosfeld, C. Mayer, A. M. Smith, J. Woodward, and N. Ross (2011), The "tipping" temperature within subglacial lake Ellsworth, West Antarctica and its implications for lake access, *Cryosphere*, *5*(3), 561–567.

Tulaczyk, S., et al. (2014), WISSARD at subglacial lake Whillans, West Antarctica: Scientific operations and initial observations, *Ann. Glaciol.*, *55*(65), 51–58.

Uribe, J. A., R. Zamora, G. Gacitúa, A. Rivera, and D. Ulloa (2014), A low power consumption radar system for measuring ice thickness and snow/firn accumulation in Antarctica, *Ann. Glaciol.*, *55*(67), 39–48, doi:10.3189/2014AoG67A055.

Vaughan, D. G., A. Rivera, J. Woodward, H. F. J. Corr, J. Wendt, and R. Zamora (2007), Topographic and hydrological controls on subglacial lake Ellsworth, West Antarctica, *Geophys. Res. Lett.*, *34*, L18501, doi:10.1029/2007GL030769.

Wright, A., and M. Siegert (2012), A fourth inventory of Antarctic subglacial lakes, *Antarct. Sci.*, *24*(6), 659–664, doi:10.1017/S095410201200048X.

Wright, A. P., M. J. Siegert, A. M. Le Brocq, and D. B. Gore (2008), High sensitivity of subglacial hydrological pathways in Antarctica to small ice-sheet changes, *Geophys. Res. Lett.*, *35*, L17504, doi:10.1029/2008GL034937.